STAT3 induces breast cancer growth via ANGPTL4, MMP13 and STC1 secretion by cancer associated fibroblasts

STAT3 induces breast cancer growth via ANGPTL4, MMP13 and STC1 secretion by Cancer Associated Fibroblasts

Lidia Avalle[1]* (ORCID: 0000-0002-5060-633X), Laura Raggi[1,2]* (ORCID: 0000-0003-0809-9909) , Emanuele Monteleone[1,3]* (ORCID: 0000-0001-7440-900X), Aurora Savino[1]* (ORCID: 0000-0002-0783-7191), Daniele Viavattene[1] (ORCID: 0000-0002-6216-3986), Luisa Statello[1,4] (ORCID: 0000-0001-8261-4214) , Andrea Camperi[1], Simona Aversano Stabile[1], Vincenzo Salemme[1], Niccolò De Marzo[1], Francesca Marino[1], Chiara Guglielmi[1,5], Andrea Lobascio[1] (ORCID: 0000-0003-0065-5931), Cristina Zanini[6] (ORCID: 0000-0002-6554-2113), Marco Forni[6], Danny Incarnato[7,8] (ORCID: 0000-0003-3944-2327), Paola Defilippi[1] (ORCID: 0000-0001-6427-4906), Salvatore Oliviero[7] (ORCID: 0000-0002-3405-765X), Valeria Poli[1] (ORCID: 0000-0002-3739-3966).

[1] Department of Molecular Biotechnology and Health Science, University of Torino, Via Nizza 52, 10126 Torino, Italy.

[2] Present address: San Raffaele-Telethon Institute for Gene Therapy (SR-TIGET), Milan, Italy.

[3] Present address: Università Vita-Salute San Raffaele, Milan, Italy.

[4] Present address: Center for Applied Medical Research, University of Navarra, Pio XII 55 Ave, 31008, Pamplona, Spain.

[5] Present address: Section of Molecular Genetics, Department of Laboratory Medicine, University Hospital of Pisa, Pisa, Italy.

[6] BioAir SPA Scientific Department, Via Nizza, 52, 10126 Torino, Italy.

[7] Department of Life Sciences and Systems Biology, University of Torino, Via Nizza 52, 10126 Torino, Italy.

[8] Present address: Department of Molecular Genetics, Groningen Biomolecular Sciences and Biotechnology Institute (GBB), University of Groningen, 9747 AG, Groningen, the Netherlands.

*Equal contributors

Corresponding authors:
Lidia Avalle, Valeria Poli, Department of Molecular Biotechnology and Health Science, University of Torino, Via Nizza 52, 10126 Torino, Italy. Phone: +39-011-6706428
Email: lidia.avalle@unito.it, valeria.poli@unito.it.

RUNNING TITLE

CAF secreted STAT3 targets sustain breast tumor progression

KEYWORDS

Cancer associated fibroblasts

STAT3

Metastasis

Breast cancer

Mouse model

Abstract

In the tumor microenvironment, Cancer Associated Fibroblasts (CAFs) become activated by cancer cells and increase their secretory activity to produce soluble factors that contribute to tumor cells proliferation, invasion and dissemination to distant organs. The pro-tumorigenic transcription factor STAT3 and its canonical inducer, the pro-inflammatory cytokine IL-6, act conjunctly in a positive feedback loop that maintains high levels of IL-6 secretion and STAT3 activation in both tumor and stromal cells. Here, we demonstrate that STAT3 is essential for the pro-tumorigenic functions of murine breast cancer CAFs both *in vitro* and *in vivo*, and identify a STAT3 signature significantly enriched for genes encoding for secreted proteins. Among these, ANGPTL4, MMP13 and STC-1 were functionally validated as STAT3-dependent mediators of CAF pro-tumorigenic functions by different approaches. Both *in vitro* and *in vivo* CAFs activities were moreover impaired by MMP13 inhibition, supporting the feasibility of a therapeutic approach based on inhibiting STAT3-induced CAF-secreted proteins. The clinical potential of such an approach is supported by the observation that an equivalent CAF-STAT3 signature in humans is expressed at high levels in breast cancer stromal cells and characterizes patients with a shorter disease specific survival, including those with basal-like disease.

Introduction

Tumor growth and dissemination to distant organs requires the support of the tumor microenvironment (TME), composed of extracellular matrix (ECM), immune and endothelial cells and fibroblasts [1], all involved in intense multidirectional communications via both cell-cell contacts and secreted molecules [1]. Cancer associated fibroblasts (CAFs), mostly derived from tissue resident fibroblasts in response to tumor molecular cues, are among the most abundant TME cell types [2]. CAF activation is triggered by ECM stiffness and composition, metabolic stress conditions and secreted signalling molecules such as TGF-β, IL-1, IL-6, and TNF [2], deriving both from tumor and infiltrating immune cells. Activated CAFs up-regulate the expression of markers such as alpha smooth muscle actin (α-SMA), vimentin, fibroblast activating protein (FAP), Platelet Derived Growth Factor (PDGFR) β, S100A4, N-cadherin and caveolin [2], and undergo metabolic reprogramming increasing aerobic glycolysis that sustains their proliferative and secretory features [3]. CAF-secreted factors enhance tumor cells growth and invasion and contribute to the development of drug resistance [3]. CAF-mediated ECM remodelling via secretion of matrix components and metalloproteinases (MMPs) also favours tissue invasion, metastasis and proliferation via shedding of mitogens from the cells surface and mobilization of ECM-embedded growth factors [4]. CAF's pro-tumorigenic activities have therefore lately attracted considerable attention as potential therapeutic targets for combination therapies [2].

The pro-oncogenic transcription factor Signal Transducer and Activator of Transcription (STAT) 3 becomes activated by tyrosine phosphorylation, mediating the signalling downstream of many cytokines and growth factor receptors [5, 6]. STAT3 is often constitutively activated in both tumor cells and the immune TME, representing a point of

convergence for numerous oncogenic signalling pathways [5]. Aberrantly activated STAT3 promotes cancer initiation and progression by inhibiting apoptosis and inducing cell proliferation [5, 7], enhancing the expression of matrix metalloproteinases, increasing matrix stiffness [8] and promoting epithelial to mesenchymal transition (EMT) [9]. Moreover, STAT3-driven secretion of soluble mediators skews the activation of infiltrating immune cells and promotes tumor angiogenesis [10]. Overexpression of constitutively active STAT3 (STAT3C) is sufficient to trigger tumor transformation of immortalized fibroblasts and epithelial cells, and primary mouse embryonic fibroblasts carrying a STAT3C mutant allele undergo a HIF-mediated metabolic switch to aerobic glycolysis and become spontaneously transformed [7, 11]. Finally, STAT3C knock-in mice develop more aggressive and metastatic breast tumors [12]. Several STAT3-regulated genes encode for cytokines and growth factors that in turn can activate the JAK-STAT3 pathway, thereby propagating a stable activation state [10]. One of the main culprits of this perverse loop is the pro-inflammatory cytokine IL-6, which can drive many of the cancer 'hallmarks' through the activation of the JAK/STAT3 signalling pathway [13]. This in turn maintains elevated IL-6 levels in a positive feedback circuit that involves both tumor and stromal cells [10]. The IL-6/JAK/STAT3 self-maintaining loop is indeed considered an important mediator of cancer onset and progression that can also be initiated by chronic inflammation, a well-known risk factor in tumorigenesis [7, 9]. Despite the many studies characterizing the role of STAT3 in both tumor and TME cells, and a number of indications that its activation is involved in breast, pancreas and liver CAF pro-tumorigenic activities [14-17], the molecular mechanisms have never been thoroughly investigated in CAFs. Here we demonstrate that STAT3 is an important mediator of CAFs pro-tumorigenic functions in mouse models of breast cancer (BC) and identify a STAT3-driven signature enriched for genes encoding for secreted proteins including Angptl1, MMP13 and Stc1. Their inhibition

significantly impairs CAF-induced tumor growth, migration and invasion both *in vitro* and *in vivo*, thus identifying them as potential therapeutic targets.

Results

STAT3 is required for *in vitro* pro-tumorigenic functions of primary CAFs.

CAFs were derived from NeuT transgenic mammary tumors [18] and analyzed for the expression of typical CAF markers along with normal and mouse embryonal fibroblasts (NFs, MEFs) (Supplementary Fig 1). Of note, most CAF markers were also expressed by NFs and even more abundantly by MEFs, suggesting how culturing can activate these cells, as already reported [2]. The only exception was S100A4, a well-recognized pro-metastatic protein[19], which expression was not detected in NFs and was significantly higher in CAFs than in MEFs. Since NFs do not therefore appear to represent an appropriate negative control, we decided to directly assess potential STAT3-dependent CAFs pro-tumorigenic functions by treating the cells with either STAT3 or control small interfering RNAs (siRNA) in a lipidoid formulation [20] (Fig. 1a, Supplementary Fig. 2 a,b). Cells were then incubated in serum-free medium for 48 hours to generate conditioned medium (CM) to treat the triple negative mouse BC cell line 4T1, followed by proliferation and migration assays. CM from siRNA control CAFs strongly enhanced 4T1 cells proliferation and migration, while STAT3 silencing significantly reduced both activities (Fig. 1b, c and Supplementary Fig. 2 c,d). Interference with STAT3 also impaired CAF-enhanced anchorage-independent proliferation of 4T1 cells, as shown by significantly smaller soft agar colonies upon seeding tumor cells in agar over a layer of CAFs (Fig. 1d, e). Moreover, CM from STAT3-silenced CAFs was significantly less effective than control in stimulating 4T1 cells extravasation (Fig. 1f). These data clearly show that STAT3 plays an important role in mediating a number of CAFs pro-tumorigenic activities.

Immortalized CAFs support *in vivo* tumor growth and rely on STAT3 activity.

In order to generate stably silenced cells for *in vivo* experiments, we established immortalized CAFs (iCAFs) via SV40 Large T Antigen expression (Supplementary Fig. 1). Similar to primary CAFs, iCAFs were able to induce 4T1 cells proliferation, migration and invasion, properties strongly impaired upon both transient siRNA and stable shRNA-mediated STAT3 silencing (Supplementary Fig. 3 a-d and Fig. 2 a-d). iCAFs were then incubated with CM from 4T1 cells in order to maximize their pro-tumorigenic power (super-activated CAFs, s.a.), resulting in enhanced pro-migratory activity (Supplementary Fig. 3e). The availability of stably silenced CAFs allowed us to perform *in vivo* experiments by co-injection with 4T1 cells into the flanks of BalbC syngeneic mice. While control CAFs strongly stimulated primary tumor growth and lung metastases, this ability was significantly blunted upon STAT3 silencing (Fig. 2e-g). Supporting the general relevance of our findings, we obtained similar results on primary tumor growth with the less aggressive BalbC murine BC cell lines TuBo [21] and TSA [22] (Supplementary Fig.4 a, c). Remarkably, CAFs co-injection elicited a dramatic increase in the number of metastatic nodules formed by these otherwise poorly metastatic cell lines (Supplementary Fig.4 b, d, compare with Fig. 2f). Different from 4T1 cells however, STAT3 silencing in CAFs did not alter the metastatic activity of TuBo cells, while a trend towards reduction was observed in the case of TSA cells.

CAFs co-injection was able to significantly enhance the growth of 4T1 primary tumors also in NSG immunocompromised mice, activity that was completely abolished when using STAT3-silenced CAFs (Supplementary Fig.4e). The metastatic burden formed by 4T1 cells in NSG mice was dramatically higher that in immunocompetent mice (compare Supplementary Fig. 4f with Figs. 2f or 6b, d), likely due to the lack of immune response.

Under these conditions, it was not possible to appreciate a further increase upon co-injection of either control or STAT3-silenced CAFs.

STAT3 gene expression signature in CAFs is enriched for genes encoding for secreted proteins.

In order to identify STAT3 transcriptional targets potentially mediating CAFs pro-oncogenic properties, we compared the mRNA expression profiles of primary CAFs silenced or not for STAT3 as obtained by RNA sequencing, and identified both up- and down-regulated genes (Supplementary Tables I and II). Down-regulated genes were enriched in Gene Ontology categories such as nucleotide metabolism, EMT, positive regulation of cell motility, regulation of inflammatory responses, T-helper Th1 response and T cell differentiation, in keeping with the predicted functions of STAT3 (Supplementary Table III). Conversely, the vast majority of up-regulated genes belonged to categories involving regulation of innate and leukocyte-mediated immune responses (Supplementary Table IV). Genes encoding for secreted proteins, potential mediators of CAFs CM activities, were significantly enriched among down-regulated mRNAs (p-value=$3.5*10^{-10}$, Fig. 3a). Differential expression of a subset of genes was confirmed by quantitative RT-PCR in independently prepared samples (Supplementary Fig. 5a). The paradigmatic STAT3 target and activator IL-6 and the genes encoding for angiopoietin-like 4 (ANGPTL4), matrix metalloproteinase 13 (MMP13) and stanniocalcin-1 (STC1) were selected for functional validation, being among the most downregulated genes carrying putative STAT3 binding sites on their regulatory regions. All four mRNAs were also significantly down-regulated in iCAFs by both siRNA and shRNA-mediated STAT3 silencing (Supplementary Fig. 5b and Fig. 3b-f). Chromatin Immunoprecipitation (ChIP) experiments clearly detected STAT3 binding to their promoter regions, confirming them as direct STAT3 transcriptional targets (Fig. 3g).

Importantly, ANGPTL4, MMP13 and IL-6 were all readily detected in the CAF supernatants and their expression reduced upon silencing, confirming them being secreted (Supplementary Fig. 6a-f, l). The failure to detect STC1 in the supernatant (Supplementary Fig. 6i) most likely reflects the poor performance of the available commercial antibodies. As it might be expected, super activation significantly increased the RNA levels of all four STAT3 targets (Supplementary Fig. 7a). Interestingly, we observed that 4T1 cells secrete about 5 times more IL-6 than iCAFs. In turn, super activation of CAFs with this IL-6 containing 4T1 CM strongly induced IL-6 production by CAFs themselves (Supplementary Fig. 7b).

4T1-secreted IL-6 is required to support pro-tumoral CAFs activities both *in vitro* and *in vivo*.

We first sought to assess the functional roles of IL-6, due to its known roles both upstream and downstream of STAT3 [5]. The induction of 4T1 cells migration triggered by iCAFs CM was significantly impaired by IL-6R blocking antibodies (Supplementary Fig. 8a). 4T1 cells were then injected with or without iCAFs in BalbC mice, followed by treatment with anti-IL-6R antibodies or control IgGs (Fig. 4a). The ability of iCAFs to enhance both primary tumor growth and lung metastasis was completely abolished by IL-6 neutralization, which did not in contrast reduce tumor growth and progression of 4T1 cells injected alone, suggesting a CAF-mediated function of IL-6 in supporting *in vivo* growth and dissemination of tumor cells (Fig. 4b, c).

We then decided to test IL-6-deficient CAFs, which were derived from IL-6-null NeuT transgenic mice. Of note, these mice displayed profoundly delayed mammary tumor onset, supporting a critical role of IL-6 (Supplementary Fig. 8b). Immortalized IL-6-null CAFs expressed similar levels of Stat3, Stc1 and Mmp13 mRNAs with respect to their wild type counterparts, and significantly higher levels of Angptl4 (Supplementary Fig. 8c). We

then co-injected IL-6-null CAFs with 4T1 cells into IL-6 deficient BalbC mice, in which 4T1 cells represent the only possible source of IL-6. In contrast to what predicted by the results obtained upon IL-6 neutralization, both wild type and IL-6 null iCAFs were similarly able to enhance primary tumor growth and lung metastases (Fig. 4 d-f), suggesting that 4T1-produced IL-6 is both necessary and sufficient to support tumor growth and progression (Supplementary Fig. 6b).

ANGPTL4, MMP13 and STC1 significantly contribute to CAFs functions.

To functionally assess the role of the other STAT3 targets ANGPTL4, MMP13 and STC1, iCAFs were stably silenced by means of lentiviral-mediated shRNAs (Fig. 5a-c), and the ability of the respective CM to enhance *in vitro* proliferation, migration or invasion of 4T1 cells was assessed. CM from sh or control iCAFs strongly stimulated the proliferation of 4T1 cells (Fig. 5 d-f), which was instead significantly reduced when CM from all shRNA-treated iCAFs was used (Fig. 5d-f). Likewise, silencing of either gene effectively impaired CM-induced 4T1 cells migration and invasion (Fig. 5 g-l).

iCAFs silenced for Angptl4, Mmp13 or Stc1 were then co-injected with 4T1 cells into BalbC mice, in order to assess their contribution to CAFs activities *in vivo*. Silencing of each of the three genes significantly impaired primary tumor growth as compared to control CAFs (Fig. 6a, c). The number and size of metastatic nodules was also strongly reduced upon Stc1 and Mmp13, but not Angptl4, silencing (Fig. 6b, d, e). In order to assess CAF-secreted proteins druggability, we took advantage of the MMP13 inhibitor WAY 170523 [23, 24]. This small molecule compound was able to significantly impair CAF-induced *in vitro* 4T1 cells invasion in a dose-dependent manner (Supplementary Fig. 9). *In vivo*, intra-tumoral delivery of the MMP13 inhibitor dose-dependently inhibited both tumor growth and metastasis formation induced by CAFs (Fig. 6f-g).

STAT3-signature genes are also relevant in human tumor stroma

To investigate the relevance of our CAF STAT3 signature in humans, we generated a human (h) CAF STAT3 signature by identifying the human ortholog genes (Supplementary Table V), and assessed their relative expression in available datasets of human primary breast tumors or micro-dissected stroma. We analyzed 32 independent primary tumor datasets derived from bulk tumor tissue, which includes both stroma and epithelium, including the well-known TCGA (The Cancer Genome Atlas) and METABRIC databases[25].

TCGA samples have been annotated for predicted stromal content using several algorithms based on either gene expression signatures, DNA methylation patterns or immunohistochemical data (see Materials and Methods). Interestingly, the expression of 68/95 hSTAT3 signature genes, including STAT3 and all our target genes with the exception of Stc-1, was positively correlated with at least 3 different stromal content predictors (Fisher-test p-value<$2.2*10^{-16}$, Fig. 7a). This observation was confirmed in 28/31 additional datasets including METABRIC, where we estimated stromal content using ssGSEA and stromal/immune signatures [26] (Supplementary Fig. 10). We also observed that the hSTAT3 signature genes are expressed at globally higher levels than the average genes in 11 microarray datasets from primary human CAFs or laser-capture micro-dissected human breast tumor stroma (Kolmogorov-Smirnov test, p-value<10^{-8}, Supplementary Table VI). This observation was further corroborated by the significantly higher expression of the hSTAT3 signature in stromal cells as compared to epithelial cells in single cell analysis of TNBC patients [27] (Fig. 7b and Supplementary Fig. 11). Genes of the hSTAT3 CAF signature are expressed at significantly higher levels in basal-like breast cancer patients, the group with worst prognosis, as compared to the other subtypes. This cannot be imputed to higher stroma abundance, since basal-like patients do not display higher stromal scores than the other

subtypes (Supplementary Fig. 12). Importantly, Disease Specific Survival was significantly reduced in patients with high expression of the hSTAT3 signature in the METABRIC cohort also taking the molecular subtype into account in a bivariate Cox model (Fig. 7c), meaning that the hSTAT3 signature correlates with survival independently of the molecular subtype.

Discussion

The pro-oncogenic transcription factor STAT3 is frequently constitutively activated in both cancer cells and the tumor stroma, in a positive feedback loop with inflammatory cytokines such as IL-6, which is a potent activator of STAT3 and, in turn, its transcriptional target. STAT3 inactivation may therefore disrupt this tumor-stroma-tumor cross-talk loop acting both on tumor and stromal cells [28]. However, lack of enzymatic activity and nuclear localization make transcription factors problematic targets for classical drugs, and indeed no STAT3 inhibitor has yet reached the clinic despite intense development efforts [28].

Our demonstration that STAT3 supports the pro-tumorigenic activities of mouse BC CAFs by inducing the production and release of soluble factors in the CM provides an alternative strategy to disrupt STAT3-mediated CAFs pro-oncogenic activities (Fig. 7d). Indeed, soluble factors can be more readily reached by inhibitors, be they small molecules or biologicals, and therefore represent ideal antitumor therapeutic targets. Accordingly, the CAF STAT3 signature was significantly enriched for secreted factors, and ANGPTL4, MMP13 and STC-1 all significantly contributed to CAFs pro-tumorigenic activity *in vitro* and *in vivo*.

The observation that IL-6 receptor blocking antibodies completely abolished CAF-activated primary tumor growth and lung metastasis development in the 4T1 xenograft model suggested at first that IL-6 is among the pro-tumorigenic STAT3-dependent CAF-secreted factors. This conclusion was however contradicted by the failure of selective IL-6 inactivation in CAFs to affect their tumor stimulating activities. These apparent contrasting results might

indicate that the IL-6 secreted by 4T1 cells mainly supports tumor growth and progression by activating CAFs. 4T1 cells produce high amounts of IL-6, which may be responsible for CAFs activation both *in vitro* and *in vivo* stimulating the expression of STAT3-dependent factors such as ANGPTL4, MMP13 and STC-1, which in turn will provide pro-tumorigenic signals to cancer cells. Our observation that anti-IL6R treatment could only reduce *in vivo* growth of 4T1 cells when co-injected with CAFs confirms that 4T1-secreted IL-6 is only relevant in the presence of CAFs, being therefore required for the tumor-to-stroma but not stroma-to-tumor cross-talk. Indeed, endogenous CAFs are likely to play a minor role in fast growing xenografted tumors, from which we repeatedly failed to isolate fibroblasts (AC and VP, unpublished observation). Importantly, several drugs targeting the IL-6-JAK-STAT3 pathway, including the anti-hIL-6R mAb Tocilizumab and several JAK inhibitors, are routinely used in the clinics and could be rapidly repurposed. However, IL-6 blockade clinical trials in ovarian and renal cancer reported only limited success [29, 30]. Considering the systemic effects of IL-6, it is possible that localized delivery of the blocking mAb, concentrating its activity in the TME and inhibiting CAF's activation, may represent a more effective strategy to inhibit the tumor-CAF-tumor cross-talk. Moreover, in the light of our results, IL-6 expression in tumor cells may serve as a stratifying marker for such an anti-IL-6 therapy.

ANGPTL4, MMP13 and STC-1 have all been reported to enhance growth and metastasis of a variety of solid tumors, and their overexpression has been observed both in cancer and in stromal cells. ANGPTL4 is a serum hormone regulating glucose homeostasis, lipid metabolism and insulin sensitivity. It was recently shown to promote brain metastasis upon BC cells injection [31], support energy production during EMT [32], and favour proliferation, migration and invasion of NSCLC cells. Interestingly, ANGPTL4 can act both downstream [33, 34] and upstream [32, 35] of STAT3 in both tumors and inflammation, and could therefore play a role in the maintenance of constitutively active STAT3. Angptl4 expression,

increased in the IL-6$^{-/-}$ CAFs, could therefore help maintaining STAT3 activity and the expression of the other STAT3 target genes, thus allowing CAFs to exert their pro-oncogenic functions. Secreted STC-1 is believed to be a paracrine/autocrine factor regulating phosphate homeostasis [36]. Its expression is often upregulated in tumors downstream of Hif1 alpha and cytokines, participating in the Warburg effect and in the EMT process and correlating with tumor growth and metastasis in BC [37]. Remarkably, STC1 expression by colorectal cancer CAFs was reported to drive metastasis via all routes (peritoneal, lymphatic and hematogenous) [38]. MMP13 was originally isolated from breast cancer and is overexpressed in a number of other solid tumors. Like other metalloproteases, it is involved in extracellular matrix remodelling, and its expression correlates with prognosis and lymph node status in BC [39-41], and with proliferation, migration, invasion and anchorage-independent growth of mouse BC tumor cells [42]. MMP13 was shown to mediate leptin/STAT3 induced migration and invasion in pancreatic adenocarcinomas, where its expression was associated with lymph node metastasis [43]. MMP13 expression was also detected in stromal cells such as myofibroblasts at the invading tumor edges [44], correlating with micro-metastasis. Our results with the MMP13 inhibitor confirm its important role in mediating pro-tumorigenic CAFs' functions and further support the idea that soluble proteins may indeed represent amenable targets to interfere with CAFs-tumor cells communications.

Although our results are derived from murine models, the analysis of human BC data suggests their relevance to the human system. Our observation that the expression of the vast majority of human STAT3-dependent CAF signature genes significantly correlates with the degree of stromal content in 29 out of 32 BC datasets analyzed strongly suggests that these genes are indeed expressed at higher level in the stroma, as also confirmed by single cell analysis. Additionally, stroma-expressed STAT3-dependent genes may contribute to the fast progression of the basal-like BC subtype, where STAT3 is often constitutively activated [45],

since these tumors express significantly higher levels of the STAT3 signature despite not differing from the other subtypes in the abundance of stromal content. Accordingly, high expression of the human STAT3 CAF signature significantly correlates with reduced survival probability in the METABRIC database. Interestingly, while our results show that STAT3 activity in CAFs is equally required for driving primary tumor growth of mouse cell lines belonging to different BC subtypes, i.e. the triple negative 4T1 [46, 47], the HER2$^+$ TuBo [21] and the ER$^+$ TSA [22], only 4T1 cells need STAT3 activity to enhance CAF-induced metastasis. These observations suggest that indeed CAFs contribution to tumor progression may be more crucial in basal-like/triple negative BC that in the other BC subtypes also in the mouse. Finally, the failure of CAFs to further increase the already dramatically high number of 4T1 cells metastasis in immunocompromised mice may suggest that, in keeping with published data [2], also in our system CAFs pro-metastatic activities are mainly related to their ability to inhibit the anti-tumor immune response [2].

In conclusion, our data demonstrate the critical role played by STAT3 in sustaining the pro-tumorigenic functions of CAFs in BC, identify the main mechanism in the induction of secreted proteins that in turn act on BC tumor cells (Fig. 7d), and prove the feasibility of inhibiting their activities *in vivo*, bypassing the hurdles of *in vivo* STAT3 inhibition.

Materials and Methods

Mice and cell lines

Mice were raised and maintained in the specific pathogen free transgenic unit of the Molecular Biotechnology Center (University of Turin) under a 12-hour light/dark cycle and provided food and water *ad libitum*. Procedures were conducted in conformity with national and international laws and policies as approved by the Faculty Ethical Committee and the Italian Ministry of health.

NeuT [18] and IL-6$^{-}/_{-}$ mice [48] were both in the BalbCA background, and were inter-crossed to obtain NeuT,IL-6$^{-}/_{-}$ or $^{+}/_{+}$ mice.

4T1 and TSA cells were purchased from ATCC and kindly provided by Prof. Mara Brancaccio, and Prof. Federica Cavallo respectively. TuBo cells were derived from a spontaneous breast tumor arisen in a female BALB/c-MMTV-NeuT mice [21] and kindly provided by Prof. Paola Defilippi. CAFs cells were cultured in high glucose complete Dulbecco's Modified Eagle's Medium (DMEM, Gibco, cat.11965092), while 4T1 and TSA cells were cultured in Roswell Park Memorial Institute 1640 Medium (RPMI + GlutaMAX^{TM}, Gibco, cat.61870010) at 37°C in a 5% CO_2 atmosphere; both media were supplemented with 10% (CAFs, TSA, and 4T1) or 20% (TuBo) heat inactivated fetal bovine serum (FBS, Gibco, cat.16000044) and 50 u/ml penicillin, 50ug/ml streptomycin (Gibco, cat.15140122). Cell lines were routinely tested to confirm the lack of mycoplasma contamination.

CAFs derivation, immortalization and silencing

CAFs were derived from mammary tumors of IL-6-sufficient or deficient NeuT transgenic mice as described below. Dissected tumors were cleaned from connective tissue and vessels, finely chopped and digested for 1h at 37°C with 1 mg/ml collagenase A (Roche, cat. 10103578001) in serum free DMEM, centrifuged for 10min at 800rpm, resuspended in 10% FBS DMEM, filtered through 70 um cell strainers and centrifuged again. The pellets were resuspended in 10% FBS DMEM and seeded for 20 minutes at 37°C, 5% CO_2. Non-adherent cells were collected and re-plated overnight, followed by differential trypsinization after 48/72 h. Primary CAFs were passaged 1:3 for a maximum of 3 passages, and frozen after the first passage, and immortalized by stable transfection with a pBABE-SV40 LargeT antigen (Addgene, cat. 1780).

Two shRNA constructs were generated for each gene in the pLKO vector (Addgene, cat.10878) (Supplementary Table VII). Lentiviral particles were produced by EffeCtene

(QIAGEN, cat. 301425) as described in http://tronolab.epfl.ch/. Supernatants were used for transduction, followed by puromycin selection (1 ug/ml) for 2 days. pLKO.1 empty vector was used as control.

Cells were treated with the siSTAT3 or control nanoparticles previously described [20], 1 ug/mL, for 72 hours.

ChIP assays

ChIP assays were performed as previously described [49] with anti-STAT3 antibodies (Cell Signaling Technology, cat. 9132, 2 ug), or rabbit IgG (LifeTech, cat. 31235). Primers for SYBR green qPCR reactions are listed in Supplementary Table VIII.

Western blots

Western blots were performed with whole protein extracts as previously described [50], with alpha-Smooth Muscle (Sigma Aldrich, cat. A5228), alpha-Tubulin (Sigma Aldrich, cat. T8203), Actin (Santa Cruz Biotechnology, cat. sc-8432), ANGPTL4 (Invitrogen, cat. 409800), Caveolin (Cell Signaling, cat. 3267), GAPDH (MilliporeSigma, cat. CB1001), IL-6 (ABclonal, cat. A0286), MMP13 (Abcam, cat. ab39012), N-cadherin (Abcam, cat. ab18203) PDGFR-β (Santa Cruz Biotechnology, cat. sc-432), S100A4 (Cell Signaling, cat. 13018), STAT3 (rabbit polyclonal raised against the carboxy-terminal region of the protein, homemade), STC-1 (Boster, cat. PA1997), Vimentin (Santa Cruz Biotechnology, cat. sc-6260), Vinculin (home-made) primary antibodies, and repeated at least three times.

RNA isolation, qRT-PCR and sequencing

Total RNA was isolated as described [50] and SYBR green qRT-PCR carried out with the primers of Supplementary Table IX.

Total TRIzol-extracted RNA from primary CAFs was subjected to quality assessment on an Agilent 2100 Bioanalyzer (RIN ≥ 9). 2 ug of total RNA were subjected to poly(A) selection. Libraries were prepared with the TruSeq RNA Sample Prep Kit (Illumina). Sequencing was

performed on the Illumina NextSeq 500 platform. Reads were mapped to the Mus musculus mm9 reference assembly using TopHat v2.0.10 (ref. http://genomebiology.com/2013/14/4/R36/abstract). Raw and processed data have been deposited to the Gene Expression Omnibus database (GSE178081). Gene counts and differential expression analysis were performed as described [50]. Only genes with FDR < 0.05 were further considered. GO enrichment of differentially expressed genes was done with the clusterProfiler package, removing not expressed genes from background (threshold: at least 1 RPKM in at least 2 samples). Genes coding for secreted proteins were selected as belonging to the Extracellular region GO category (GO:0005576).

Conditioned medium and CAFs super-activation

Conditioned medium was obtained by plating $2x10^6$ CAFs in a 100 mm diameter dish, followed after 24 hours by 48h incubation with serum free medium, filtered (0.22 um) and used to treat 4T1 cells for 48h, followed by functional assays. iCAFs were super-activated for 48 hours with 4T1-conditioned medium prepared in the same way.

Transwell and proliferation assays

Transwell assays for 4T1 cells were performed with $1x10^5$ 4T1 cells using 8 um pore Transwell inserts (Falcon, cat.353097), coated or not with Matrigel matrix (Corning, cat.354480), against 1% FBS DMEM in the lower chamber. After 16h (migration), or 24h (invasion), migrated cells were quantified as described [50]. Anti-mouse IL-6R (rat MAb 15A7 clone) or control IgG (Thermo Fisher Scientific, cat. 31933), 50 ug/ml, were added to the CM.

Proliferation: $4x10^3$ 4T1 cells pre-treated with CM were seeded in 96-well plates in triplicate, CM supplemented with 2% FBS was provided after 4h and replaced every other day. Quantifications were performed upon Crystal Violet staining (0.1%) followed by 10% acetic acid elution and 600 nm absorbance measurement.

Scratch assay and anchorage independent growth

In vitro scratch assays were performed as previously described [50]. Images (6 fields per experiment) were taken after 24h with a phase contrast Olympus IX70 microscope.

For anchorage independent growth, CAFs were seeded in 24 well plates and treated with STAT3 siRNA or controls for 72h, then overlaid with a suspension of $4x10^3$ 4T1 cells in complete DMEM and 0.3% low gelling agarose (Sigma Aldrich, cat. A9045). After 2 weeks colonies were stained and counted as described [50].

Extravasation, $5x10^5$ CM-treated 4T1 cells were labelled with CellTracker Orange CMRA (Thermo Fisher Scientific), resuspended in PBS and injected into the tail vein of BalbC mice. Mice were sacrificed and intratracheally perfused with 4% paraformaldehyde. Lungs were dissected and imaged as described [50].

***In vivo* tumor growth and spontaneous metastasis assays**

In vivo tumorigenesis: $3x10^5$ super-activated iCAFs were co-injected bilaterally with $1x10^5$ 4T1 cells in the flank of 6 weeks old syngeneic female BalbC. Tumors were caliper-measured at the indicated time points, and the volume was calculated as (length x $width^2$)/2. After 10 days primary tumors were surgically removed, and mice sacrificed at day 21 for lung metastasis evaluation, upon intratracheal perfusion with 4% paraformaldehyde. Lungs were formalin-fixed, paraffin-embedded, and semi-serial sections were stained and imaged as described [50]. Metastatic lesions were quantified with the ImageJ software.

aIL-6R (rat MAb 15A7 clone) or control IgG (500 ug/mouse) was injected intraperitoneally every three days starting from the day before cells injection, until day 10. The MMP13 inhibitor WAY 170523 (Tocris, cat. 2633) was used as described in [23].

Public gene expression data

TCGA data were from https://portal.gdc.cancer.gov/, METABRIC data from http://synapse.org/ (syn1757063), and additional breast cancer transcriptome datasets were

obtained from package MetaGxBreast [51] (only datasets with at least 10000 probes). Stroma-related datasets were downloaded from Gene Expression Omnibus as pre-normalized expression matrices (Supplementary Table VI, part of the MetaLCM database[52]). All gene IDs were converted to HGNC symbols, and in case of more probes mapping to the same gene, the probe with the highest mean expression across dataset's samples was kept. Data were log scaled before further analyses.

Estimate of stromal percentage

Pre-computed stromal percentage estimates were available for TCGA: EDEc data were downloaded from http://genboree.org/theCommons/documents/569, Stromal scores from https://bioinformatics.mdanderson.org/estimate/disease.html (RNASeqV2), and Tumor purity data from TCGAbiolinks [53]. For the additional datasets, percentage of stroma was computed as in [26] making use of the GSVA package [54] for ssGSEA.

Human STAT3 CAFs signature expression and survival analysis

METABRIC's Disease Specific Survival data were downloaded from http://synapse.org/ (syn1757055). Human orthologs of the mouse STAT3 signature genes were inferred as the uppercase versions of mouse IDs, signature expression was computed for each METABRIC sample with ssGSEA making use of the GSVA package [54] , and the Cox model was obtained with the coxph function from the survival R package (https://CRAN.R-project.org/package=survival) taking into account both signature expression and PAM50 tumor subtype, and represented with the ggforest function from the survminer R package (Kassambara A., Kosinski M and Biecek P.(2020). survminer: Drawing Survival Curves using 'ggplot2'). The single cell dataset GSE118390 [27] was processed using the Seurat R package [55] for normalization, scaling and clustering. Single cells were clustered based on the expression of the most variable genes. Cell type was attributed to clusters using cell type

markers supplied in [27]. The expression of Stat3 signature was compared between epithelial and stromal cells.

Statistical analysis

Unless otherwise noted, data were analyzed by Prism8 (GraphPad software) and presented as mean±S.E.M of the indicated number of samples. The specific test used to determine statistical significance is indicated in the figure legend of each experiment. Briefly, cell proliferation and tumor growth experiments were analysed by 2 way-ANOVA with Bonferroni post-test. As non-parametric tests the two-tailed Mann Whitney *U* test (when only 2 conditions were present), or the Kruskal-Wallis test (more than 2 conditions), followed by Uncorrected Dunn's test for comparison between two indicated groups, were used. Enrichment was calculated with the fisher.test R function (one tailed), correlation and its significance with the cor.test function, and Kolmogorov-Smirnov test with the ks.test function.

References

1. Joyce, J.A. and J.W. Pollard, *Microenvironmental regulation of metastasis.* Nat Rev Cancer, 2009. **9**(4).
2. Sahai, E., I. Astsaturov, E. Cukierman, D.G. DeNardo, M. Egeblad, R.M. Evans, et al., *A framework for advancing our understanding of cancer-associated fibroblasts.* Nat Rev Cancer, 2020. **20**(3).
3. Kalluri, R., *The biology and function of fibroblasts in cancer.* Nat Rev Cancer, 2016. **16**(9).
4. Lynch, C.C. and L.M. Matrisian, *Matrix metalloproteinases in tumor-host cell communication.* Differentiation, 2002. **70**(9-10).
5. Avalle, L., A. Camporeale, A. Camperi, and V. Poli, *STAT3 in cancer: A double edged sword.* Cytokine, 2017. **98**.
6. Avalle, L., S. Pensa, G. Regis, F. Novelli, and V. Poli, *STAT1 and STAT3 in tumorigenesis: A matter of balance.* JAKSTAT, 2012. **1**(2).
7. Demaria, M., S. Misale, C. Giorgi, V. Miano, A. Camporeale, J. Campisi, et al., *STAT3 can serve as a hit in the process of malignant transformation of primary cells.* Cell Death Differ, 2012. **19**(8).
8. Laklai, H., Y.A. Miroshnikova, M.W. Pickup, E.A. Collisson, G.E. Kim, A.S. Barrett, et al., *Genotype tunes pancreatic ductal adenocarcinoma tissue tension to induce matricellular fibrosis and tumor progression.* Nat Med, 2016. **22**(5).
9. Yu, H., D. Pardoll, and R. Jove, *STATs in cancer inflammation and immunity: a leading role for STAT3.* Nat Rev Cancer, 2009. **9**(11).
10. Yu, H., M. Kortylewski, and D. Pardoll, *Crosstalk between cancer and immune cells: role of STAT3 in the tumour microenvironment.* Nat Rev Immunol, 2007. **7**(1).
11. Demaria, M., C. Giorgi, M. Lebiedzinska, G. Esposito, L. D'Angeli, A. Bartoli, et al., *A STAT3-mediated metabolic switch is involved in tumour transformation and STAT3 addiction.* Aging (Albany NY), 2010. **2**(11).
12. Barbieri, I., E. Quaglino, D. Maritano, T. Pannellini, L. Riera, F. Cavallo, et al., *Stat3 is required for anchorage-independent growth and metastasis but not for mammary tumor development downstream of the ErbB-2 oncogene.* Mol Carcinog, 2010. **49**(2).
13. Wang, S.W. and Y.M. Sun, *The IL-6/JAK/STAT3 pathway: potential therapeutic strategies in treating colorectal cancer (Review).* Int J Oncol, 2014. **44**(4).
14. Albrengues, J., T. Bertero, E. Grasset, S. Bonan, M. Maiel, I. Bourget, et al., *Epigenetic switch drives the conversion of fibroblasts into proinvasive cancer-associated fibroblasts.* Nat Commun, 2015. **6**.
15. Hendrayani, S.F., H.H. Al-Khalaf, and A. Aboussekhra, *The cytokine IL-6 reactivates breast stromal fibroblasts through transcription factor STAT3-dependent up-regulation of the RNA-binding protein AUF1.* J Biol Chem, 2014. **289**(45).
16. Yang, X., Y. Lin, Y. Shi, B. Li, W. Liu, W. Yin, et al., *FAP Promotes Immunosuppression by Cancer-Associated Fibroblasts in the Tumor Microenvironment via STAT3-CCL2 Signaling.* Cancer Res, 2016. **76**(14).
17. Zheng, X., M. Xu, B. Yao, C. Wang, Y. Jia, and Q. Liu, *IL-6/STAT3 axis initiated CAFs via up-regulating TIMP-1 which was attenuated by acetylation of STAT3 induced by PCAF in HCC microenvironment.* Cell Signal, 2016. **28**(9).
18. Barbieri, I., S. Pensa, T. Pannellini, E. Quaglino, D. Maritano, M. Demaria, et al., *Constitutively active Stat3 enhances neu-mediated migration and metastasis in mammary tumors via upregulation of Cten.* Cancer Res, 2010. **70**(6).
19. Boye, K. and G.M. Maelandsmo, *S100A4 and metastasis: a small actor playing many roles.* Am J Pathol, 2010. **176**(2).

20. Avalle, L., F. Marino, A. Camporeale, C. Guglielmi, D. Viavattene, S. Bandini, et al., *Liver-Specific siRNA-Mediated Stat3 or C3 Knockdown Improves the Outcome of Experimental Autoimmune Myocarditis.* Mol Ther Methods Clin Dev, 2020. **18**.
21. Rovero, S., A. Amici, E. Di Carlo, R. Bei, P. Nanni, E. Quaglino, et al., *DNA vaccination against rat her-2/Neu p185 more effectively inhibits carcinogenesis than transplantable carcinomas in transgenic BALB/c mice.* J Immunol, 2000. **165**(9).
22. Nanni, P., C. de Giovanni, P.L. Lollini, G. Nicoletti, and G. Prodi, *TS/A: a new metastasizing cell line from a BALB/c spontaneous mammary adenocarcinoma.* Clin Exp Metastasis, 1983. **1**(4).
23. Quillard, T., Y. Tesmenitsky, K. Croce, R. Travers, E. Shvartz, K.C. Koskinas, et al., *Selective inhibition of matrix metalloproteinase-13 increases collagen content of established mouse atherosclerosis.* Arterioscler Thromb Vasc Biol, 2011. **31**(11).
24. Yu, H., A. Fellows, K. Foote, Z. Yang, N. Figg, T. Littlewood, et al., *FOXO3a (Forkhead Transcription Factor O Subfamily Member 3a) Links Vascular Smooth Muscle Cell Apoptosis, Matrix Breakdown, Atherosclerosis, and Vascular Remodeling Through a Novel Pathway Involving MMP13 (Matrix Metalloproteinase 13).* Arterioscler Thromb Vasc Biol, 2018. **38**(3).
25. Curtis, C., S.P. Shah, S.F. Chin, G. Turashvili, O.M. Rueda, M.J. Dunning, et al., *The genomic and transcriptomic architecture of 2,000 breast tumours reveals novel subgroups.* Nature, 2012. **486**(7403).
26. Yoshihara, K., M. Shahmoradgoli, E. Martinez, R. Vegesna, H. Kim, W. Torres-Garcia, et al., *Inferring tumour purity and stromal and immune cell admixture from expression data.* Nat Commun, 2013. **4**.
27. Karaayvaz, M., S. Cristea, S.M. Gillespie, A.P. Patel, R. Mylvaganam, C.C. Luo, et al., *Unravelling subclonal heterogeneity and aggressive disease states in TNBC through single-cell RNA-seq.* Nat Commun, 2018. **9**(1).
28. Huynh, J., A. Chand, D. Gough, and M. Ernst, *Therapeutically exploiting STAT3 activity in cancer - using tissue repair as a road map.* Nat Rev Cancer, 2019. **19**(2).
29. Dijkgraaf, E.M., S.J. Santegoets, A.K. Reyners, R. Goedemans, M.C. Wouters, G.G. Kenter, et al., *A phase I trial combining carboplatin/doxorubicin with tocilizumab, an anti-IL-6R monoclonal antibody, and interferon-alpha2b in patients with recurrent epithelial ovarian cancer.* Ann Oncol, 2015. **26**(10).
30. Rossi, J.F., S. Negrier, N.D. James, I. Kocak, R. Hawkins, H. Davis, et al., *A phase I/II study of siltuximab (CNTO 328), an anti-interleukin-6 monoclonal antibody, in metastatic renal cell cancer.* Br J Cancer, 2010. **103**(8).
31. Gong, X., Z. Hou, M.P. Endsley, E.I. Gronseth, K.R. Rarick, J.M. Jorns, et al., *Interaction of tumor cells and astrocytes promotes breast cancer brain metastases through TGF-beta2/ANGPTL4 axes.* NPJ Precis Oncol, 2019. **3**.
32. Teo, Z., M.K. Sng, J.S.K. Chan, M.M.K. Lim, Y. Li, L. Li, et al., *Elevation of adenylate energy charge by angiopoietin-like 4 enhances epithelial-mesenchymal transition by inducing 14-3-3gamma expression.* Oncogene, 2017. **36**(46).
33. Garner, J.M., D.W. Ellison, D. Finkelstein, D. Ganguly, Z. Du, M. Sims, et al., *Molecular heterogeneity in a patient-derived glioblastoma xenoline is regulated by different cancer stem cell populations.* PLoS One, 2015. **10**(5).
34. Li, L., H.C. Chong, S.Y. Ng, K.W. Kwok, Z. Teo, E.H.P. Tan, et al., *Angiopoietin-like 4 Increases Pulmonary Tissue Leakiness and Damage during Influenza Pneumonia.* Cell Rep, 2015. **10**(5).
35. Chong, H.C., J.S. Chan, C.Q. Goh, N.V. Gounko, B. Luo, X. Wang, et al., *Angiopoietin-like 4 stimulates STAT3-mediated iNOS expression and enhances angiogenesis to accelerate wound healing in diabetic mice.* Mol Ther, 2014. **22**(9).

36. Zhao, F., G. Yang, M. Feng, Z. Cao, Y. Liu, J. Qiu, et al., *Expression, function and clinical application of stanniocalcin-1 in cancer.* J Cell Mol Med, 2020. **24**(14).
37. Chang, A.C., J. Doherty, L.I. Huschtscha, R. Redvers, C. Restall, R.R. Reddel, et al., *STC1 expression is associated with tumor growth and metastasis in breast cancer.* Clin Exp Metastasis, 2015. **32**(1).
38. Pena, C., M.V. Cespedes, M.B. Lindh, S. Kiflemariam, A. Mezheyeuski, P.H. Edqvist, et al., *STC1 expression by cancer-associated fibroblasts drives metastasis of colorectal cancer.* Cancer Res, 2013. **73**(4).
39. Folgueira, M.A., S. Maistro, M.L. Katayama, R.A. Roela, F.G. Mundim, S. Nanogaki, et al., *Markers of breast cancer stromal fibroblasts in the primary tumour site associated with lymph node metastasis: a systematic review including our case series.* Biosci Rep, 2013. **33**(6).
40. Paek, A.R., J.Y. Mun, K.M. Hong, J. Lee, D.W. Hong, and H.J. You, *Zinc finger protein 143 expression is closely related to tumor malignancy via regulating cell motility in breast cancer.* BMB Rep, 2017. **50**(12).
41. Zhang, B., X. Cao, Y. Liu, W. Cao, F. Zhang, S. Zhang, et al., *Tumor-derived matrix metalloproteinase-13 (MMP-13) correlates with poor prognoses of invasive breast cancer.* BMC Cancer, 2008. **8**.
42. Dumortier, M., F. Ladam, I. Damour, S. Vacher, I. Bieche, N. Marchand, et al., *ETV4 transcription factor and MMP13 metalloprotease are interplaying actors of breast tumorigenesis.* Breast Cancer Res, 2018. **20**(1).
43. Fan, Y., Y. Gan, Y. Shen, X. Cai, Y. Song, F. Zhao, et al., *Leptin signaling enhances cell invasion and promotes the metastasis of human pancreatic cancer via increasing MMP-13 production.* Oncotarget, 2015. **6**(18).
44. Nielsen, B.S., F. Rank, J.M. Lopez, M. Balbin, F. Vizoso, L.R. Lund, et al., *Collagenase-3 expression in breast myofibroblasts as a molecular marker of transition of ductal carcinoma in situ lesions to invasive ductal carcinomas.* Cancer Res, 2001. **61**(19).
45. Tell, R.W. and C.M. Horvath, *Bioinformatic analysis reveals a pattern of STAT3-associated gene expression specific to basal-like breast cancers in human tumors.* Proc Natl Acad Sci U S A, 2014. **111**(35).
46. Aslakson, C.J. and F.R. Miller, *Selective events in the metastatic process defined by analysis of the sequential dissemination of subpopulations of a mouse mammary tumor.* Cancer Res, 1992. **52**(6).
47. Schrors, B., S. Boegel, C. Albrecht, T. Bukur, V. Bukur, C. Holtstrater, et al., *Multi-Omics Characterization of the 4T1 Murine Mammary Gland Tumor Model.* Front Oncol, 2020. **10**.
48. Poli, V., R. Balena, E. Fattori, A. Markatos, M. Yamamoto, H. Tanaka, et al., *Interleukin-6 deficient mice are protected from bone loss caused by estrogen depletion.* EMBO J, 1994. **13**(5).
49. Vallania, F., D. Schiavone, S. Dewilde, E. Pupo, S. Garbay, R. Calogero, et al., *Genome-wide discovery of functional transcription factor binding sites by comparative genomics: the case of Stat3.* Proc Natl Acad Sci U S A, 2009. **106**(13).
50. Avalle, L., D. Incarnato, A. Savino, M. Gai, F. Marino, S. Pensa, et al., *MicroRNAs-143 and -145 induce epithelial to mesenchymal transition and modulate the expression of junction proteins.* Cell Death Differ, 2017. **24**(10).
51. Gendoo, D.M.A., M. Zon, V. Sandhu, V.S.K. Manem, N. Ratanasirigulchai, G.M. Chen, et al., *MetaGxData: Clinically Annotated Breast, Ovarian and Pancreatic Cancer Datasets and their Use in Generating a Multi-Cancer Gene Signature.* Sci Rep, 2019. **9**(1).

52. Savino, A., N. De Marzo, P. Provero, and V. Poli, *Meta-Analysis of Microdissected Breast Tumors Reveals Genes Regulated in the Stroma but Hidden in Bulk Analysis.* Cancers (Basel), 2021. **13**(13).
53. Colaprico, A., T.C. Silva, C. Olsen, L. Garofano, C. Cava, D. Garolini, et al., *TCGAbiolinks: an R/Bioconductor package for integrative analysis of TCGA data.* Nucleic Acids Res, 2016. **44**(8).
54. Hanzelmann, S., R. Castelo, and J. Guinney, *GSVA: gene set variation analysis for microarray and RNA-seq data.* BMC Bioinformatics, 2013. **14**.
55. Stuart, T., A. Butler, P. Hoffman, C. Hafemeister, E. Papalexi, W.M. Mauck, 3rd, et al., *Comprehensive Integration of Single-Cell Data.* Cell, 2019. **177**(7).

Acknowledgments

The authors wish to thank D. Taverna, C. Ambrogio, E. Calautti, M. Mazzone for critically reading the manuscript. This work was supported by the Italian Cancer Research Association (AIRC, IG16930 to V.P.; IG 20240 to S.O.); the Italian Ministry of University and Research (MIUR PRIN 2017 to V.P.); the Truus and Gerrit van Riemsdijk Foundation, Liechtenstein, donation to V.P.; Piedmont Region (Deflect). L. Avalle was supported by Fondazione Umberto Veronesi.

Author contributions

Conception, design and study supervision VP; bioinformatics data generation and analysis, EM, AS, NDM, DI, SO; *in vitro* experiments, AC, CG, FM, SAS, LR, DV, AL, DI; *in vivo* experiments, LA, AC, LR, DV, SAS, VS; Acquisition of data, CZ and MF; Analysis and interpretation of data, EM, LA, AS, LR, DV, DI, VP, PD, SO.

Conflict of interest

The authors declare that they have no conflict of interest.

Figure legends

Figure 1. STAT3 is required for CAFs pro-tumorigenic functions.

a. Schematic representation of the experimental setting. Primary CAFs derived from BalbC/NeuT mice were transiently silenced for STAT3 (siS3, red) or not (siC, black). Conditioned medium (CM) from these cells was used to treat 4T1 tumor cells, followed by proliferation, migration, anchorage independent growth and extravasation assays, together with untreated 4T1 cells (-, grey). **b.** 4T1 cells proliferation was measured by crystal violet staining, and shown as mean±S.E.M of the O.D. of each sample relative to day 0, n=3. **c.** Transwell migration assay, mean±S.E.M of migrated cells relative to controls (siC), n=6. Representative images stained with crystal violet, scale bar: 100 um. **d, e.** Soft agar colony assay. 4T1 cells were seeded on a layer of the indicated CAFs. Data are mean±S.E.M of colony number (d) and size (e), n=8. Representative colony images are shown, scale bar: 20 um. **f.** Extravasation assay. Fluorescently labeled 4T1 cells, pretreated *in vitro* with the indicated CAFs CM for 48h, were injected i.v. into BalbC mice. Lungs were collected after 2 hours, to assess equal loading, and at 24 hours to measure extravasation. Data are expressed as number of cells/field, each dot representing the mean of 4 independent fields per mouse, n=10. Representative images of fluorescently labeled cells into the lungs, at the indicated times after i.v. injection, are shown.

p-values were calculated by 2-way ANOVA in b, by Kruskal-Wallis test in c, f (P value<0.0001) followed by Uncorrected Dunn's test for the indicated comparisons, or by Mann-Whitney *U* test in d, e. ****, p<0.0001; ***, p<0.001; *, p<0.05; ns, not significant.

Figure 2. Immortalized CAFs show STAT3 dependent pro-tumorigenic features both *in vitro* and *in vivo*.

a. Immortalized CAFs (iCAFs) were stably transduced with lentiviral shRNA either control (shC, black) or against STAT3 (shS3, teal), and silencing was assessed by qRT-PCR and Western blot. Data are mean±S.E.M of Stat3 mRNA expression normalized on TBP and relative to control (shC), n=9. Their CM was used to treat 4T1 cells, followed by functional assays as described for Figure 1. **b.** Cell proliferation. Data are mean±S.E.M. of the O.D. of each sample relative to day 0, n=6. **c, d.** Transwell migration (c, n=8) and invasion (d, n=6) assays, shown as mean±S.E.M. of migrated cells relative to control cells (shC). Representative images upon crystal violet staining are shown, scale bar: 100 um. **e-g.** 4T1 cells were s.c. co-injected with the indicated iCAFs at a 1:3 ratio. **e.** Primary tumors were measured at the indicated days after injection, and data are shown as mean±S.E.M. of the tumor volume (-, grey, 4T1 cells only, n=12; shC, black, 4T1 cells + iCAFs shC, n=8; shS3, teal, 4T1 cells + iCAFs shS3, n=10). **f, g.** Lungs were dissected at day 21, fixed and H&E stained. The metastatic area was quantified as described in the Materials and Methods section, and expressed as percentage of the total lung area (mean±S.E.M., -, grey, 4T1 cells only, n=5; shC, black, 4T1 cells + iCAFs shC, n=8; shS3, teal, 4T1 cells + iCAFs shS3, n=10). Representative images upon H&E staining are shown in g, scale bar: 1 mm. p-values were calculated by Mann-Whitney *U* test in a, c, d, by 2-way ANOVA in b, e, by Kruskal-Wallis test in f (P value = 0.0009), followed by Uncorrected Dunn's test for the indicated comparisons. ****, $p<0.0001$; ***, $p<0.001$; **, $p<0.01$, *, $p<0.05$.

Figure 3. STAT3 regulates the expression of several CAF-secreted proteins.

a. Differential gene expression between CAFs silenced or not for STAT3 by means of siRNA treatment was determined by RNA sequencing. The table shows statistically significant downregulated genes encoding for secreted proteins, with an asterisk indicating those validated by qRT-PCR (see Supplementary Fig. 5). **b-f.** The expression of STAT3 and of the

indicated target genes was analyzed by qRT-PCR in iCAFs transduced with lentiviral vectors carrying shRNA either control (shC, black) or against STAT3 (shS3, teal), n=6. **g.** *In vivo* binding of STAT3 to the promoters of the indicated genes was assessed by ChIP with anti-STAT3 antibodies in shC or shS3 iCAFs, followed by qPCR analysis. STAT3 binding is expressed as fold enrichment relative to IgG immunoprecipitation, upon normalization with total input, n=3. All data are mean±S.E.M of values for each group. p-values were calculated by Mann-Whitney *U* test, ***, $p<0.001$; **, $p<0.01$; *, $p<0.05$.

Figure 4. IL-6 blockade impairs CAFs ability to support *in vivo* growth of 4T1 cells

a-c. *In vivo* growth of 4T1-iCAFs cells co-injected into wild type BalbC mice. **a.** 4T1 cells were co-injected or not with iCAFs into BalbC mice, followed by i.p. treatments with anti-IL-6R mAb (aIL-6R, green) or control IgG (black) every 3 days, starting the day before tumor cells inoculation. **b.** Primary tumors were measured at the indicated days after injection, n=10. **c.** Lung metastases were evaluated 21 days after injection as described for Figure 1, and the metastatic area quantified, n=4-5. **d-f.** *In vivo* growth of 4T1-iCAFs, either wild type or IL-$6^{-/-}$, co-injected into IL-$6^{-/-}$ BalbC mice. **d.** 4T1 cells were co-injected with IL-$6^{+/+}$ or IL-$6^{-/-}$ iCAFs, in IL-$6^{-/-}$ BalbC mice. **e.** Primary tumors were measured at the indicated days after injection, n=30. **f.** Lung metastases were evaluated after 21 days after injection as described above; -, 4T1 cells alone, n=17; IL-$6^{+/+}$, n= 23; IL-$6^{-/-}$, n= 11. Data are shown as mean tumor volume±S.E.M. (b, e), or as metastatic area ±S.E.M (c, f). p-values were calculated by 2-way ANOVA test (b, e), or with Kruskal-Wallis test in c, f (c, P value = 0.1744; f, P value = 0.116) followed by Uncorrected Dunn's test for the indicated comparisons. Representative lung H&E images are shown, scale bar: 1 mm. ****, $p<0.0001$; ***, $p<0.001$; **, $p<0.01$; *, $p<0.05$; ns, not significant.

Figure 5. Angptl4, MMP13 and Stc1 mediate *in vitro* CAFs pro-tumorigenic functions.

iCAFs were stably transduced with two independent shRNAs against ANGPTL4 (left column), MMP13 (central column) and STC1 (right column), as indicated, or with a control shRNA (shC) followed by: **a-c.** assessment of the expression levels by qRT-PCR. Data are mean±S.E.M of the indicated mRNA expression, normalized on TBP and relative to control (shC), n=6-8. **d-f.** Cell proliferation of 4T1 cells upon 48h incubation with the CM from the indicated iCAF lines, or with serum free medium (-). Graphs represent mean±S.E.M. of O.D. normalized to day 0, n=8. **g-l.** Transwell migration (g-i) and invasion (j-l) of 4T1 cells pretreated with the indicated CM. Graphs show the mean±S.E.M. of migrated/invading cells relative to controls, n= 6-9. p-values were calculated by Kruskal-Wallis test (a-c, P value=0.0003; g, h, P value<0.0001; i, P value=0.0259; j, P value=0.0002; k, P value=0.0009; l, P value=0.0004), followed by Uncorrected Dunn's test for the indicated comparisons, or by 2-way ANOVA in d-f.

****, p<0.0001; ***, p<0.001; **, p<0.01; *, p<0.05; ns, not significant. Representative images of crystal violet stained Transwells are shown, scale bar 100 um.

Figure 6. Stc1 and Mmp13 strongly contribute to CAF-induced 4T1 tumors growth and progression.

The indicated sh iCAFs were co-injected with 4T1 cells into BalbC mice, followed by primary tumors and lung metastases evaluation. **a, c.** Primary tumors were measured at the indicated days after injection. a, Stc1 and MMP13 silencing; b, Angptl4 silencing. p-values were calculated by 2-way ANOVA (n=22). **b, d,** Lung metastases were evaluated after 21 days from the injection, in mice co-injected either with control iCAFs (black; b, n=17; d, n=10), or with iCAFs silenced for MMP13 (b, blue, n=15), Stc1 (b, STC1, purple, n=7), or Angptl4 (d, orange, n=11). The metastatic area was quantified upon H&E staining (**e**),

normalized on total lung area and expressed as a percentage of lung section. p-values were calculated by Kruskal-Wallis test in b, P value<0.0001, followed by Uncorrected Dunn's test for the indicated comparisons, or by Mann-Whitney *U* test in d. Representative lung H&E images are shown (e), scale bar: 1 mm. **f, g.** WT iCAFs were co-injected with 4T1 cells into BalbC mice, and intratumorally injected every 3 days with MMP13 inhibitor (0,5 mg/kg, pale blue, n=5; 1 mg/kg, blue, n=5), or with vehicle as a control (black, n=10). **f.** Primary tumors were measured at the indicated days. p-value was calculated by global ANOVA. **g.** Lung metastases were evaluated 27 days after injection as described for panels b, d, e. Data are mean±S.E.M. of each group, p-value was calculated by Kruskal-Wallis test, P value=0.0139, followed by Dunn's test for comparisons with vehicle. ****, p<0.0001; ***, p<0,001; **, p<0,01; *, p<0,05; ns, not significant.

Figure 7. The CAF STAT3 signature is conserved in human breast cancer stroma and correlates with poor survival.

a. Heatmap showing the correlation between genes in the hSTAT3 signature and the stromal percentage in TCGA, as estimated with 4 independent algorithms. EDec (Epigenomic Deconvolution of stromal percentage), STROMAL (based on gene expression profiles), ABSOLUTE (based on somatic copy-number data), IHC (haematoxylin and eosin staining). Red indicates highly positive Pearson's correlation, blue negative correlation, grey non-significant correlation. Genes without sufficient significant correlations could not be clustered and were removed. **b.** The violin plots show the human STAT3 signature expression (width, expression density; inner boxplots, expression median and lower/upper quartiles) in single-cell RNA-seq data from TNBC patients, grouped by cell type (epithelial or stromal), as defined by the expression of a list of marker genes. **c.** The hSTAT3 signature correlates with poor survival, as shown by the Forest plot of the Cox model obtained on the METABRIC

cohort, taking into account the ssGSEA score of the hSTAT3 gene signature for each patient and the molecular subtype stratification. **d.** Model of the pro-tumorigenic roles of STAT3 and its druggable secreted targets in CAFs. IL-6 secreted by primary tumor cells activates CAFs, inducing STAT3-dependent induction of a set of genes encoding for secreted proteins including the functionally characterized Angptl4, MMP13 and Stc1 (tumor-to-stroma cross-talk). Those in turn exert pro-proliferative, pro-migratory and pro-invasive functions on tumor cells, enhancing the growth of the primary tumor and the formation of lung metastases. The silencing of the characterized target genes in CAFs or the inhibition of the functions of their encoded, secreted proteins impair the pro-tumorigenic actions of CAFs.

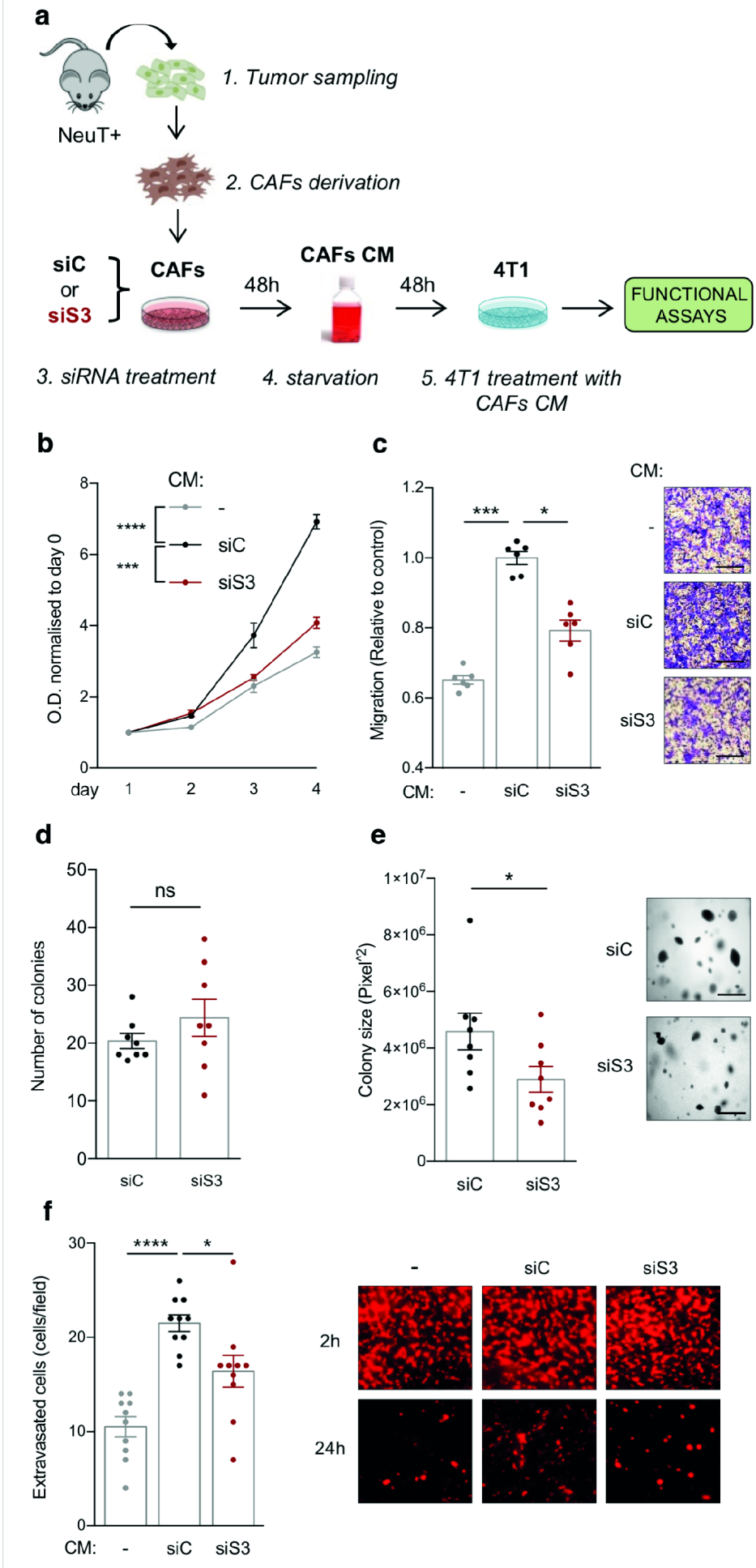
a
1. Tumor sampling
NeuT+
2. CAFs derivation
siC
or
siS3
CAFs
48h
CAFs CM
48h
4T1
FUNCTIONAL ASSAYS
3. siRNA treatment
4. starvation
5. 4T1 treatment with CAFs CM
b
CM:
-
siC
siS3
****
***
O.D. normalised to day 0
day
c
CM:
***
*
Migration (Relative to control)
d
ns
Number of colonies
e
*
Colony size (Pixel^2)
f
****
*
Extravasated cells (cells/field)
2h
24h

Figure 1

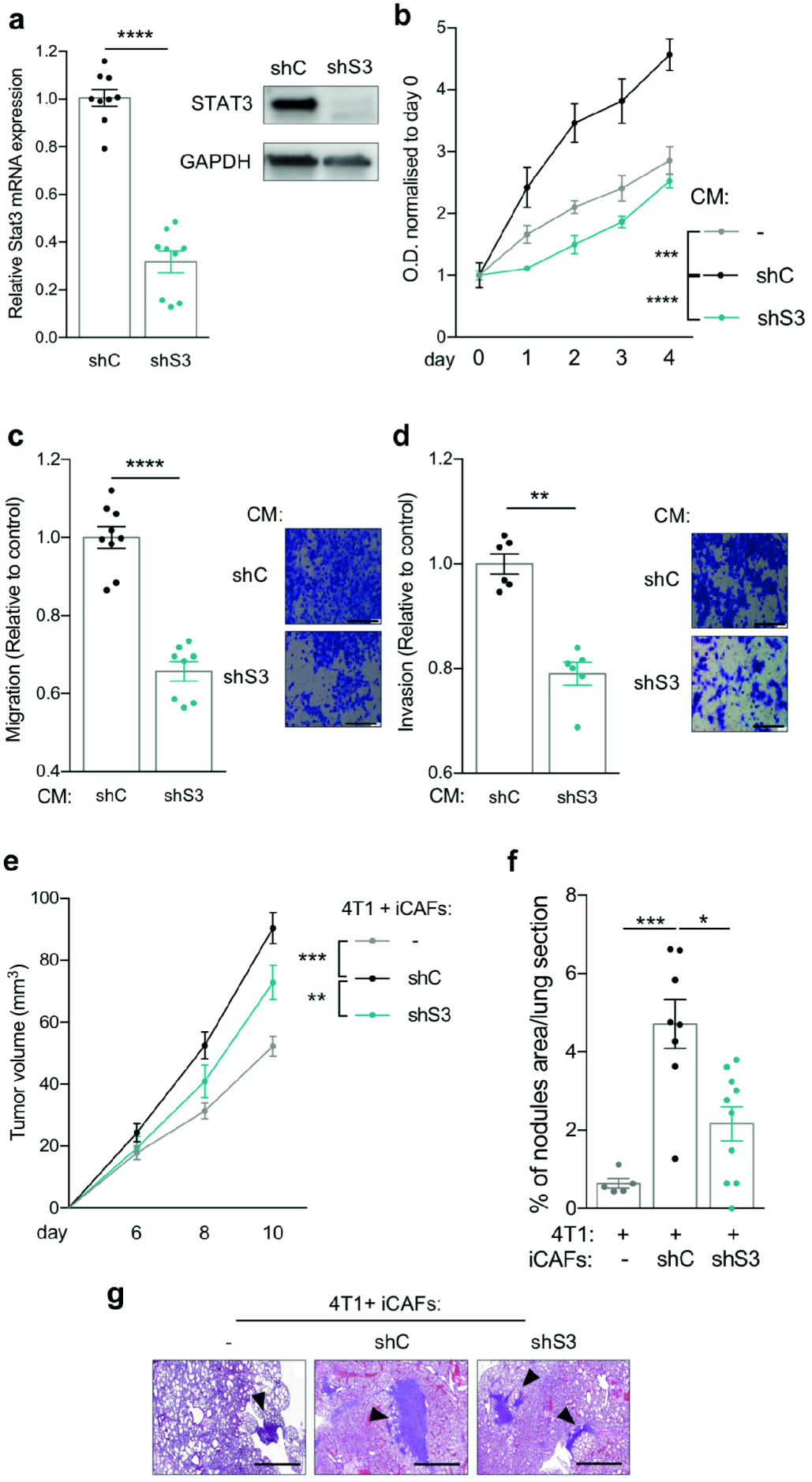
a
****
Relative Stat3 mRNA expression
1.2
1.0
0.8
0.6
0.4
0.2
0.0
shC
shS3
shC
shS3
STAT3
GAPDH
b
O.D. normalised to day 0
5
4
3
2
1
0
day 0 1 2 3 4
CM:
-
shC
shS3
***
****
c
****
Migration (Relative to control)
1.2
1.0
0.8
0.6
0.4
CM: shC shS3
CM:
shC
shS3
d
**
Invasion (Relative to control)
1.2
1.0
0.8
0.6
CM: shC shS3
CM:
shC
shS3
e
Tumor volume (mm3)
100
80
60
40
20
0
day 6 8 10
4T1 + iCAFs:
-
shC
shS3
***
**
f
***
*
% of nodules area/lung section
8
6
4
2
0
4T1: + + +
iCAFs: - shC shS3
g
4T1+ iCAFs:
-
shC
shS3

Figure 2

a

Gene	log2FC	Adj. P value	
Serpinb2	2,71	1,38E-25	*
Il6	1,18	1,46E-09	*
Angptl4	1,24	2,40E-07	*
Stc1	1,70	9,03E-07	*
Ndrg1	1,00	5,09E-05	
Mmp13	1,72	8,77E-05	*
Rtn4rl2	1,83	1,58E-04	
Slc2a1	0,63	2,64E-04	
Vegfa	0,70	3,80E-04	*
Il33	1,35	3,87E-04	*
Apln	2,40	4,14E-04	
Col24a1	1,15	6,08E-04	
Lgi2	1,53	8,47E-04	
Steap4	1,64	8,70E-04	
Clca2	1,70	8,87E-04	
Gbe1	0,77	9,00E-04	
Cp	0,77	1,48E-03	
Lbp	1,48	1,55E-03	
Draxin	2,12	1,61E-03	
Lcn2	0,62	1,81E-03	
Arrdc4	0,63	2,48E-03	
Timp1	0,52	2,48E-03	*
Cfh	1,12	2,60E-03	*
Ism1	1,08	3,34E-03	
Ndrg2	0,73	3,97E-03	
Chl1	2,58	5,24E-03	
Eno2	0,72	5,29E-03	
Mmp3	1,85	6,44E-03	*
Il1r1	0,84	8,32E-03	
Slpi	0,83	9,29E-03	
Nt5e	0,83	9,32E-03	
Cxcl14	0,78	1,10E-02	
Xpnpep2	1,98	1,34E-02	
Ampd3	0,61	1,50E-02	
Angptl2	0,65	1,52E-02	
Tnn	1,36	2,09E-02	
C3	0,84	2,18E-02	
Cxcl1	0,74	2,18E-02	
Alpl	1,12	2,47E-02	
Sdc4	0,49	2,75E-02	
Sema6d	1,36	3,06E-02	
Il17ra	0,66	3,11E-02	
Slc16a1	0,79	3,53E-02	
Heg1	0,78	3,53E-02	
Cxcl3	0,91	3,74E-02	*
Wfdc2	0,84	4,70E-02	*
Sod2	0,51	4,72E-02	

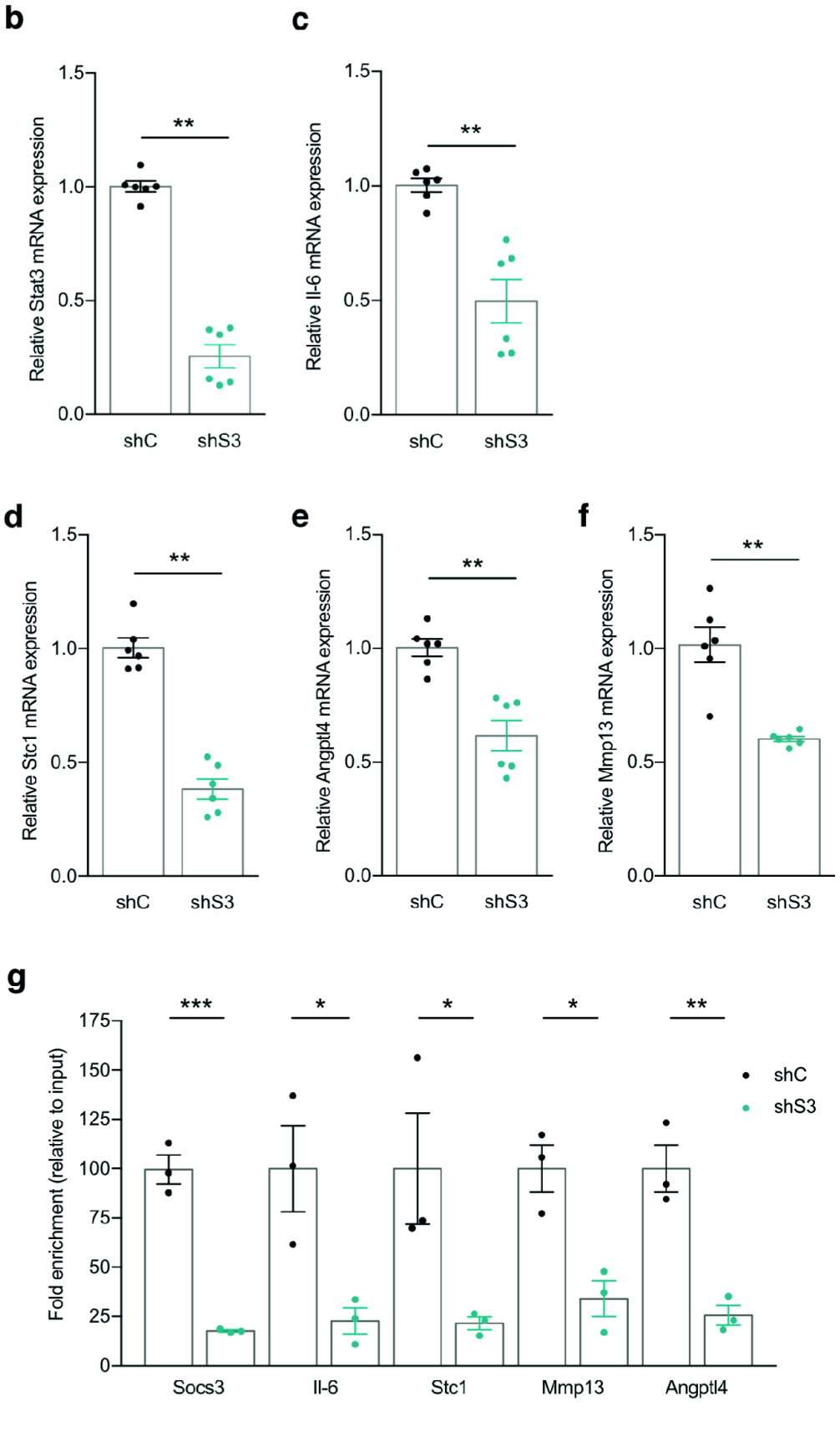

Figure 3

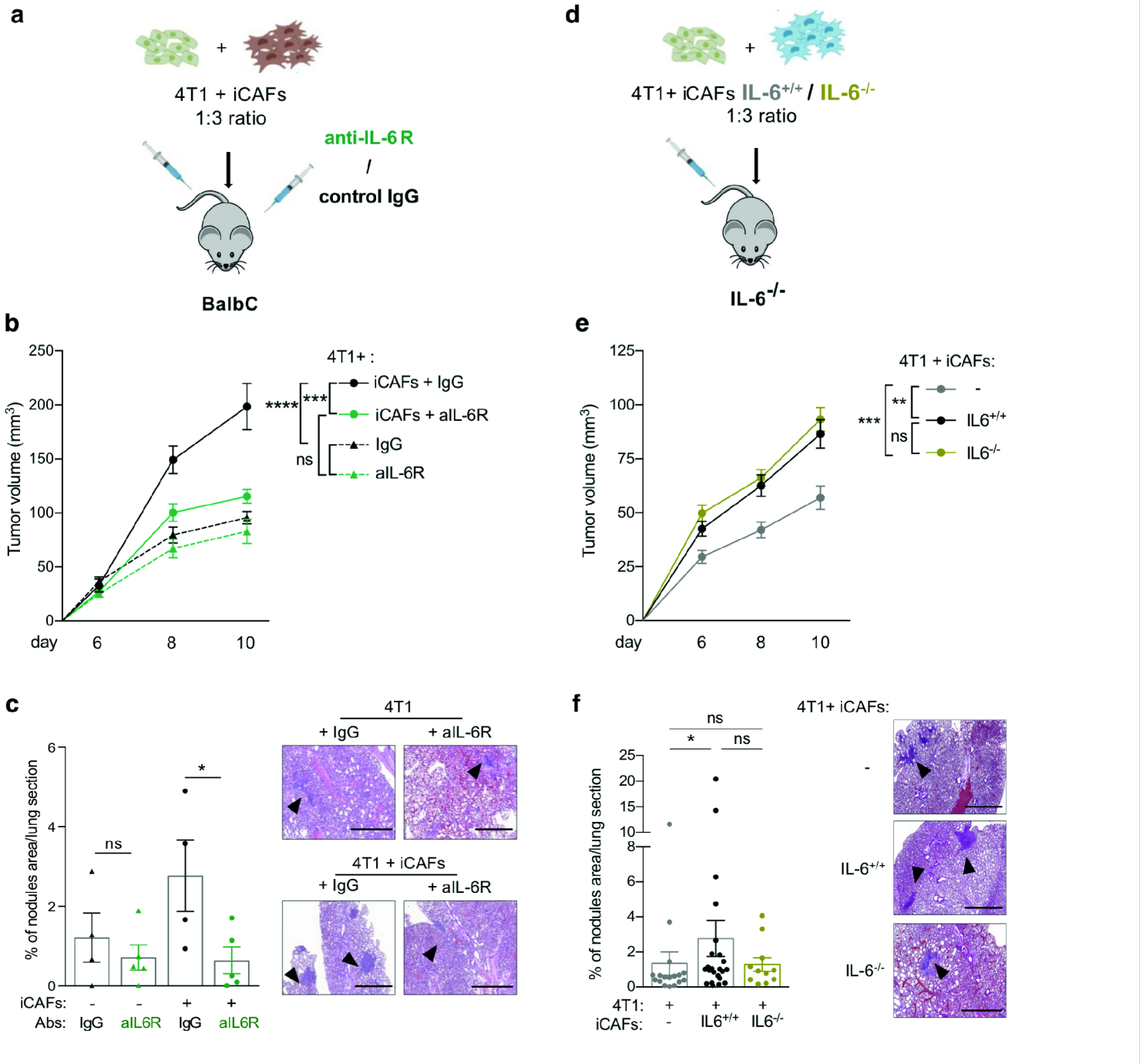
a
4T1 + iCAFs
1:3 ratio
anti-IL-6 R
/
control IgG
BalbC
d
4T1+ iCAFs IL-6+/+ / IL-6-/-
1:3 ratio
IL-6-/-
b
Tumor volume (mm3)
day
4T1+ :
iCAFs + IgG
iCAFs + aIL-6R
IgG
aIL-6R
****
***
ns
e
Tumor volume (mm3)
day
4T1 + iCAFs:
-
IL6+/+
IL6-/-
**
***
ns
c
% of nodules area/lung section
iCAFs:
Abs:
IgG
aIL6R
ns
*
4T1
+ IgG
+ aIL-6R
4T1 + iCAFs
f
% of nodules area/lung section
4T1:
iCAFs:
IL6+/+
IL6-/-
ns
*
4T1+ iCAFs:
IL-6+/+
IL-6-/-

Figure 4

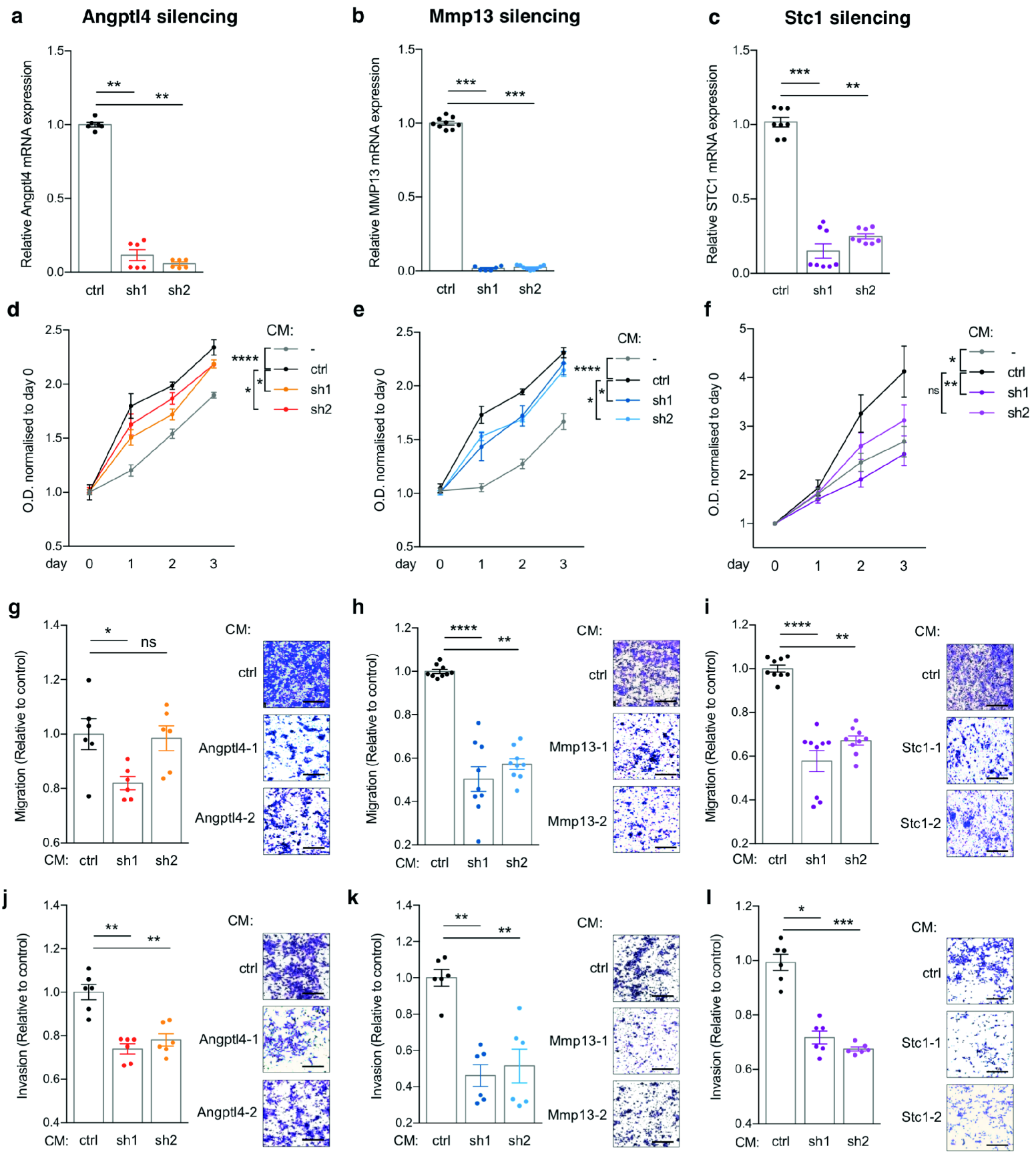
a
Angptl4 silencing
Relative Angptl4 mRNA expression
ctrl
sh1
sh2
b
Mmp13 silencing
Relative MMP13 mRNA expression
c
Stc1 silencing
Relative STC1 mRNA expression
d
e
f
O.D. normalised to day 0
day
CM:
-
ctrl
sh1
sh2
g
h
i
Migration (Relative to control)
Angptl4-1
Angptl4-2
Mmp13-1
Mmp13-2
Stc1-1
Stc1-2
ns
j
k
l
Invasion (Relative to control)

Figure 5

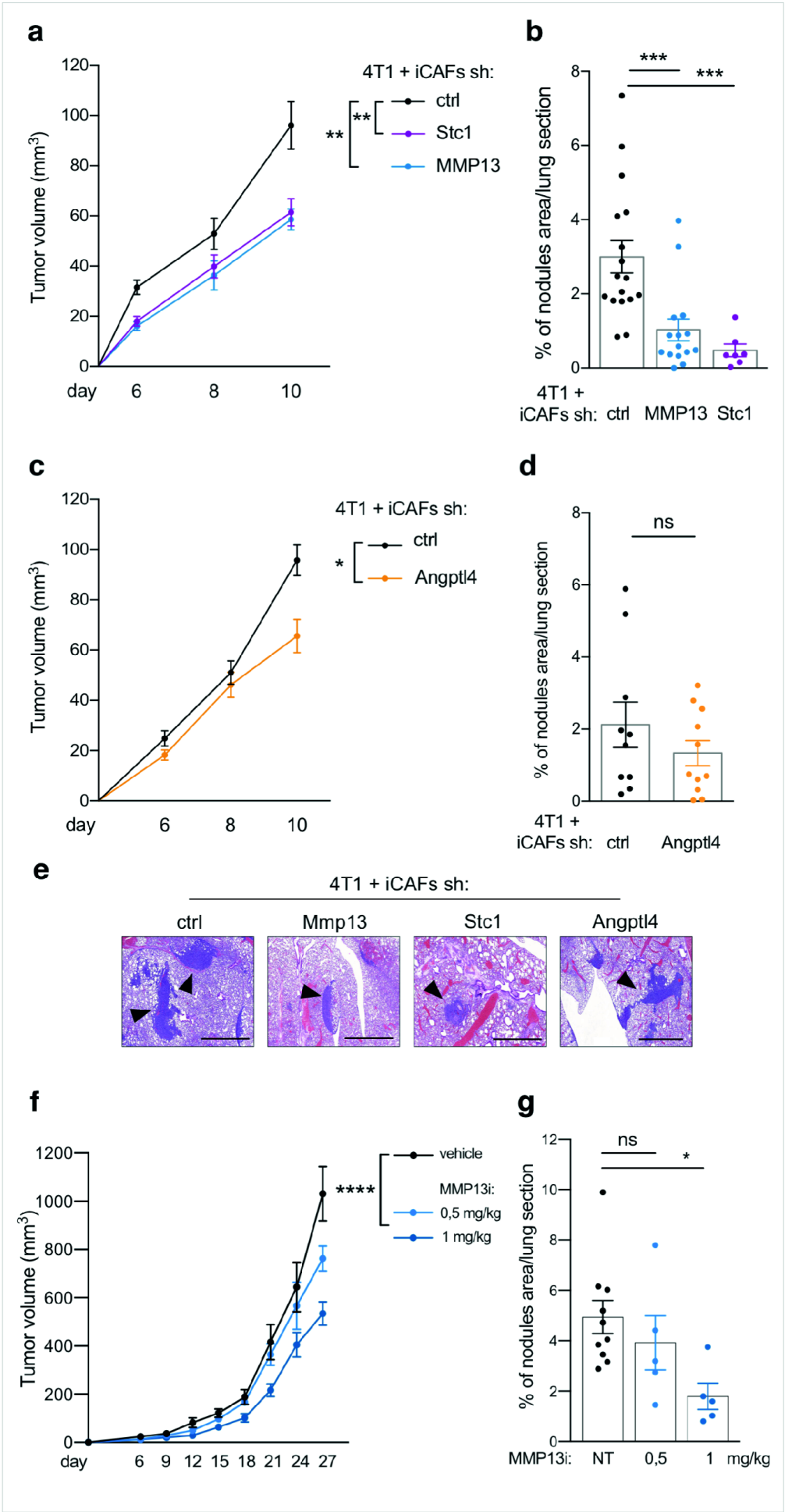
a
Tumor volume (mm3)
day
4T1 + iCAFs sh:
ctrl
Stc1
MMP13
**
**
b
% of nodules area/lung section
***
***
4T1 + iCAFs sh: ctrl MMP13 Stc1
c
Tumor volume (mm3)
day
4T1 + iCAFs sh:
ctrl
Angptl4
*
d
% of nodules area/lung section
ns
4T1 + iCAFs sh: ctrl Angptl4
e
4T1 + iCAFs sh:
ctrl
Mmp13
Stc1
Angptl4
f
Tumor volume (mm3)
day
vehicle
MMP13i:
0,5 mg/kg
1 mg/kg
****
g
% of nodules area/lung section
ns
*
MMP13i: NT 0,5 1 mg/kg

Figure 6

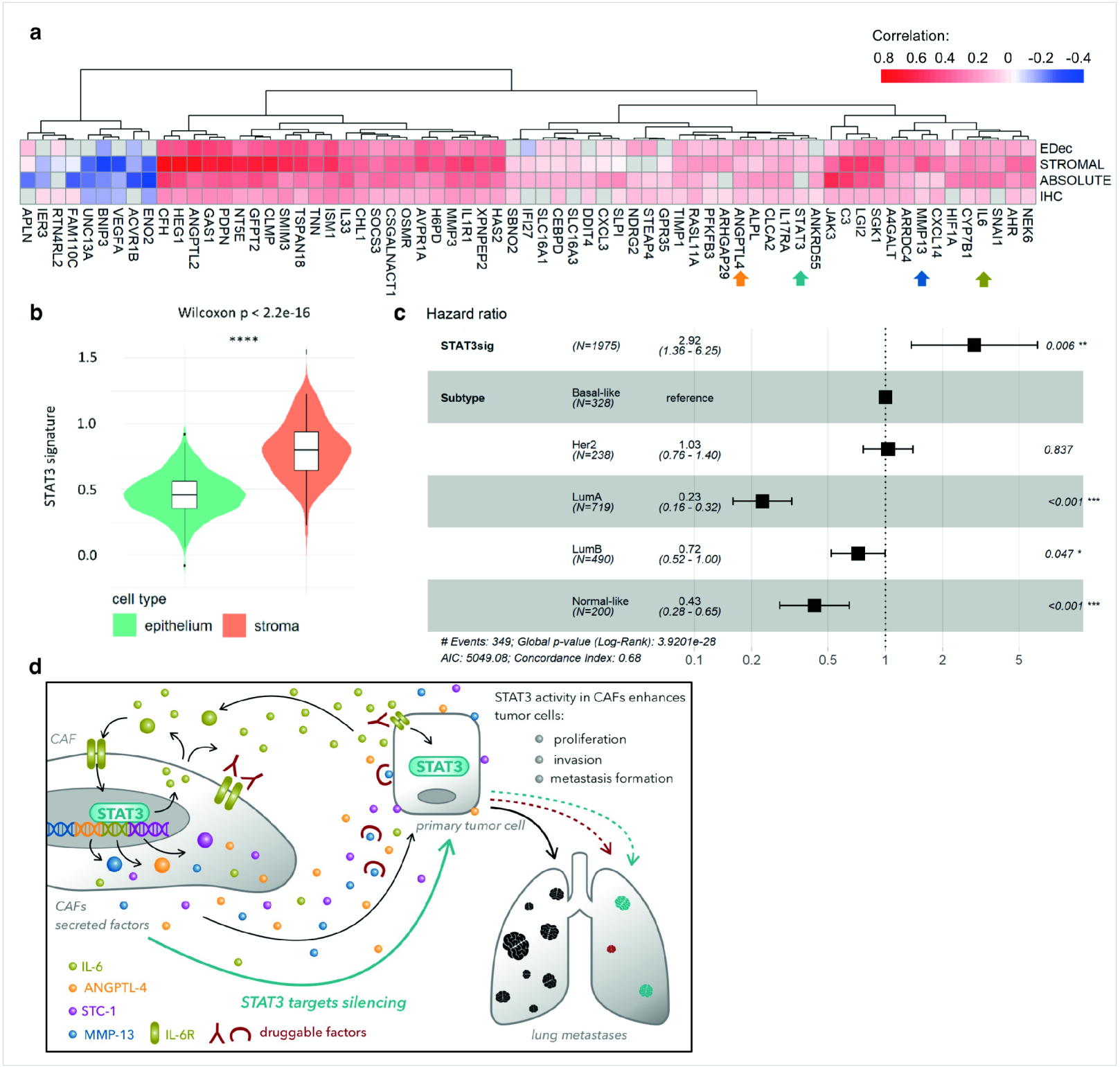
a
Correlation:
0.8 0.6 0.4 0.2 0 -0.2 -0.4
EDec
STROMAL
ABSOLUTE
IHC
APLN IER3 RTN4RL2 FAM110C UNC13A BNIP3 VEGFA ACVR1B ENO2 CFH HEG1 ANGPTL2 GAS1 PDPN GFPT2 CLMP SMIM3 TSPAN18 TNN ISM1 IL33 CHL1 SOCS3 CSGALNACT1 OSMR AVPR1A H6PD MMP3 IL1R1 XPNPEP2 HAS2 SBNO2 IFI27 SLC16A1 CEBPD SLC16A3 DDIT4 CXCL3 SLPI NDRG2 STEAP4 GPR35 TIMP1 RASL11A PFKFB3 ARHGAP29 ANGPTL4 ALPL CLCA2 IL17RA STAT3 ANKRD55 JAK3 C3 LGI2 SGK1 A4GALT ARRDC4 MMP13 CXCL14 HIF1A CYP7B1 IL6 SNAI1 AHR NEK6
b
Wilcoxon p < 2.2e-16
****
STAT3 signature
1.5
1.0
0.5
0.0
cell type
epithelium
stroma
c
Hazard ratio
STAT3sig (N=1975) 2.92 (1.36 - 6.25) 0.006 **
Subtype
Basal-like (N=328) reference
Her2 (N=238) 1.03 (0.76 - 1.40) 0.837
LumA (N=719) 0.23 (0.16 - 0.32) <0.001 ***
LumB (N=490) 0.72 (0.52 - 1.00) 0.047 *
Normal-like (N=200) 0.43 (0.28 - 0.65) <0.001 ***
Events: 349; Global p-value (Log-Rank): 3.9201e-28
AIC: 5049.08; Concordance Index: 0.68
0.1 0.2 0.5 1 2 5
d
CAF
STAT3
STAT3
primary tumor cell
CAFs
secreted factors
IL-6
ANGPTL-4
STC-1
MMP-13
IL-6R
druggable factors
STAT3 targets silencing
STAT3 activity in CAFs enhances tumor cells:
proliferation
invasion
metastasis formation
lung metastases

Figure 7